



**HAL**  
open science

## Rapid recovery of life at ground zero of the end-Cretaceous mass extinction

Christopher Lowery, Timothy Bralower, Jeremy Owens, Francisco Rodríguez-Tovar, Heather Jones, Jan Smit, Michael Whalen, Phillippe Claeys, Kenneth Farley, Sean Gulick, et al.

► **To cite this version:**

Christopher Lowery, Timothy Bralower, Jeremy Owens, Francisco Rodríguez-Tovar, Heather Jones, et al.. Rapid recovery of life at ground zero of the end-Cretaceous mass extinction. *Nature*, 2018, 558 (7709), pp.288 - 291. 10.1038/s41586-018-0163-6 . hal-01849424

**HAL Id: hal-01849424**

<https://hal.umontpellier.fr/hal-01849424v1>

Submitted on 26 Apr 2024

**HAL** is a multi-disciplinary open access archive for the deposit and dissemination of scientific research documents, whether they are published or not. The documents may come from teaching and research institutions in France or abroad, or from public or private research centers.

L'archive ouverte pluridisciplinaire **HAL**, est destinée au dépôt et à la diffusion de documents scientifiques de niveau recherche, publiés ou non, émanant des établissements d'enseignement et de recherche français ou étrangers, des laboratoires publics ou privés.



Published in final edited form as:

*Nature*. 2018 June ; 558(7709): 288–291. doi:10.1038/s41586-018-0163-6.

## Rapid Recovery of Life at Ground Zero of the End Cretaceous Mass Extinction

Christopher M. Lowery<sup>1,\*</sup>, Timothy J. Bralower<sup>2</sup>, Jeremy D. Owens<sup>3</sup>, Francisco J. Rodríguez-Tovar<sup>4</sup>, Heather Jones<sup>2</sup>, Jan Smit<sup>5</sup>, Michael T. Whalen<sup>6</sup>, Phillipe Claeys<sup>7</sup>, Kenneth Farley<sup>8</sup>, Sean P. S. Gulick<sup>1</sup>, Joanna V. Morgan<sup>9</sup>, Sophie Green<sup>10</sup>, E. Chenot<sup>11</sup>, G. L. Christeson<sup>1</sup>, C. S. Cockell<sup>12</sup>, M. J. L. Coolen<sup>13</sup>, L. Ferrière<sup>14</sup>, C. Gebhardt<sup>15</sup>, K. Goto<sup>16</sup>, D. A. Kring<sup>17</sup>, J. Lofi<sup>18</sup>, R. Ocampo-Torres<sup>19</sup>, L. Perez-Cruz<sup>20</sup>, A. E. Pickersgill<sup>21,22</sup>, M. H. Poelchau<sup>23</sup>, A. S. P. Rae<sup>9</sup>, C. Rasmussen<sup>1</sup>, M. Rebolledo-Vieyra<sup>24</sup>, U. Riller<sup>25</sup>, H. Sato<sup>26</sup>, S. M. Tikoo<sup>27</sup>, N. Tomioka<sup>28</sup>, J. Urrutia-Fucugauchi<sup>20</sup>, J. Vellekoop<sup>7</sup>, A. Wittmann<sup>29</sup>, L. Xiao<sup>30</sup>, K. E. Yamaguchi<sup>31,32</sup>, and W. Zylberman<sup>33</sup>

<sup>1</sup>Institute for Geophysics, Jackson School of Geosciences, University of Texas at Austin, USA

<sup>2</sup>Department of Geosciences, Pennsylvania State University, University Park, USA <sup>3</sup>Department

of Earth, Ocean and Atmospheric Science | National High Magnetic Field Laboratory, Florida

State University, Tallahassee, FL 32306, USA <sup>4</sup>Departamento de Estratigrafía y Paleontología,

Universidad de Granada, 18002 Granada, Spain <sup>5</sup>Faculty of Earth and Life Sciences (FALW),

Vrije Universiteit Amsterdam, Netherlands <sup>6</sup>Department of Geosciences, University of Alaska

Fairbanks, USA <sup>7</sup>Analytical, Environmental and Geo-Chemistry, Vrije Universiteit Brussel,

Brussels, Belgium <sup>8</sup>Division of Geological and Planetary Sciences, MS 170-25, California Institute

of Technology Pasadena, CA 91125, USA <sup>9</sup>Department of Earth Science and Engineering,

Imperial College London, UK <sup>10</sup>British Geological Survey, Edinburgh, UK <sup>11</sup>Biogéosciences

Laboratory, Université de Bourgogne-Franche Comté, Dijon, France <sup>12</sup>UK Centre for Astrobiology,

School of Physics and Astronomy, University of Edinburgh, Edinburgh, UK <sup>13</sup>School of Earth and

Planetary Sciences, WA-Organic and Isotope Geochemistry Centre (WA-OIGC), Curtin

University, Bentley, Australia <sup>14</sup>Natural History Museum, Vienna, Austria <sup>15</sup>Alfred Wegener

Institute Helmholtz Centre of Polar and Marine Research, Bremerhaven, Germany <sup>16</sup>International

Research Institute of Disaster Science, Tohoku University, Sendai, Japan <sup>17</sup>Lunar and Planetary

Institute, Houston, USA <sup>18</sup>Géosciences Montpellier, CNRS, Université de Montpellier, France

<sup>19</sup>Groupe de Physico-Chimie de l'Atmosphère, L'Institut de Chimie et Procédés pour l'Énergie,

Users may view, print, copy, and download text and data-mine the content in such documents, for the purposes of academic research, subject always to the full Conditions of use: [http://www.nature.com/authors/editorial\\_policies/license.html#terms](http://www.nature.com/authors/editorial_policies/license.html#terms) Reprints and permissions information is available at [www.nature.com/reprints](http://www.nature.com/reprints).

\*Correspondence and requests for materials should be addressed to CML ([cmlowery@utexas.edu](mailto:cmlowery@utexas.edu)).

**Data Availability Statement:** XRF data are published the IODP *Proceedings* volume for Expedition 364 (<https://doi.org/10.14379/iodp.proc.364.2017>). The authors declare that all other data supporting the findings of this study are available within the paper and its supplementary information files.

Supplementary Information is linked to the online version of the paper at [www.nature.com/nature](http://www.nature.com/nature).

**Author Contributions** All authors participated in sampling and data collection offshore and/or onshore during IODP/ICDP Expedition 364. CML, TJB, FJR, HJ, and JS collected and analyzed microfossil data, MTW provided detailed sedimentology, JDO, PC, and KF collected trace element, XRF, and He isotope data, respectively. All authors contributed to writing/editing of the manuscript.

The authors declare no competing financial interests.

l'Environnement et la Santé (ICPEES), Université de Strasbourg, France <sup>20</sup>Instituto de Geofísica, Universidad Nacional Autónoma De México, Ciudad de México, México <sup>21</sup>School of Geographical and Earth Sciences, University of Glasgow, UK <sup>22</sup>Argon Isotope Facility, Scottish Universities Environmental Research Centre (SUERC), East Kilbride, UK <sup>23</sup>Department of Geology, University of Freiburg, Germany <sup>24</sup>SM 312, Mza 7, Chipre 5, Resid. Isla Azul, Cancun, Quintana Roo, México, 77500 <sup>25</sup>Institut für Geologie, Universität Hamburg, Germany <sup>26</sup>Ocean Resources Research Center for Next Generation, Chiba Institute of Technology, Chiba, Japan <sup>27</sup>Earth and Planetary Sciences, Rutgers University, New Brunswick, USA <sup>28</sup>Kochi Institute for Core Sample Research, Japan Agency for Marine-Earth Science and Technology, Kochi, Japan <sup>29</sup>LeRoy Eyring Center for Solid State Science, Physical Sciences, Arizona State University, Tempe, USA <sup>30</sup>Planetary Science Institute, School of Earth Sciences, China University of Geosciences (Wuhan), China <sup>31</sup>Department of Chemistry, Toho University, Chiba, Japan <sup>32</sup>NASA Astrobiology Institute, USA <sup>33</sup>CNRS, Institut pour la Recherche et le Développement, Aix Marseille University, France

## Abstract

The Cretaceous-Paleogene (K-Pg) mass extinction eradicated 76% of species on Earth<sup>1,2</sup>. It was caused by the impact of an asteroid<sup>3,4</sup> on the Yucatán carbonate platform in the southern Gulf of Mexico at 66.0 Ma<sup>5</sup> which formed the Chicxulub impact crater<sup>6,7</sup>. Following the mass extinction, recovery of the global marine ecosystem, measured in terms of primary productivity, was geographically heterogeneous<sup>8</sup>, as export production in the Gulf of Mexico and North Atlantic/Tethys took 300 kyr to return to Late Cretaceous quantities, slower than most other regions<sup>8–11</sup>. Delayed recovery of marine productivity closer to the crater implies an impact-related environmental control, like toxic metal poisoning<sup>12</sup>, on recovery times. Conversely, if no such geographic pattern exists, the best explanation for the observed heterogeneity is ecological, based on trophic interactions<sup>13</sup>, species incumbency and competitive exclusion by opportunists<sup>14</sup>, and “chance”<sup>8,15,16</sup>. Importantly, this question has bearing on the inherent predictability (or lack thereof) of future patterns of recovery in modern anthropogenically perturbed ecosystems. If there is a relationship between the distance from the impact and the recovery of marine productivity, we would expect recovery rates to be slowest in the crater itself. Here, we present the first record of foraminifera, calcareous nannoplankton, trace fossils, and elemental abundance data from the first ~200 kyr of the Paleocene within the Chicxulub Crater. We show that life reappeared in the basin just years after the impact and a thriving, high-productivity ecosystem was established within 30 kyr, faster than many sites across the globe. This is a clear indication that proximity to the impact did not delay recovery and thus there was no impact-related environmental control on recovery. Ecological processes likely controlled the recovery of productivity after the K-Pg mass extinction and are therefore likely to be significant in the response of the ocean ecosystem to other rapid extinction events.

---

The recent joint Expedition 364 of the International Ocean Discovery Program and International Continental Drilling Program recovered the first record of the few hundred thousand years immediately after the impact within the Chicxulub Crater. Site M0077, drilled into the crater’s peak ring<sup>7</sup> (Extended Data Fig. 1), sampled a ~130 m thick generally

upward-fining suevite (i.e., melt-bearing impact breccia) overlying impact melt rocks and fractured granite<sup>17</sup>. The boundary between the suevite and overlying earliest Paleocene pelagic limestone is in Core 40-1 (Fig. 1), and is comprised of a 76 cm upward-fining, brown, fine-grained, micritic limestone that we term the transitional unit. The lower portion of the transitional unit is laminated below 54 cm core depth and contains no trace fossils (Fig. 1, Extended Data Fig. 2). The laminations are thin graded beds with sub-mm scale cross bedding that indicate bottom currents and are likely due to the movement of wave energy, including tsunamis and/or seiches, in the days after the impact. The fine grain size (primarily clay to silt, with some sand-sized grains concentrated in the graded beds) suggests that much of the material in the transitional unit was deposited from resuspension and settling. The transitional unit is overlain by a white pelagic limestone. The lowermost sample taken in this limestone (34 cm) contains the planktic foraminifer *Parvularugolobigerina eugubina*, which marks the base of Zone Pa, as well as *P. extensa*, *P. alabamensis*, and *Guembelitria cretacea*. Because many other species that originate within Zone Pa first appear a few cm higher in the section (31–32 cm), we conclude that the base of the limestone lies very near the base of this zone, 30 kyr post-impact<sup>18</sup>.

Biostratigraphy and basic assumptions about depositional and crater processes indicate that the transitional unit was deposited between several years and 30 kyr after impact (Fig. 2). To better constrain this, we utilize the abundance of extraterrestrial <sup>3</sup>He to determine sediment accumulation rates (see Methods). This proxy provides a firm upper limit of 8 kyr for deposition, assuming none of the <sup>3</sup>He is reworked. If even a small amount of <sup>3</sup>He is reworked (very likely, given the prevalence of reworked microfossils and impact debris), then the transitional unit was deposited in a period of time below the resolution of the method, < ~1 kyr. With no sediment source other than settling of material suspended by the impact and subsequent tsunamis and seiches, a more realistic estimate for the duration of this unit is based on Stoke's law, which suggests ~6 years for the settling of a 2 μm grain of carbonate (an upper limit, as most grains are much larger; see SI for further discussion). The lower portion of the overlying limestone, which contains fossils which appear ~30 kyr post impact, appears conformable with the transitional unit and must therefore be condensed due to low pelagic sedimentation in the first few 10s of kyrs post impact.

Clear, discrete trace fossils, including *Planolites* and *Chondrites*, characterize the upper 20 cm of the transitional unit (above 54 cm) (Fig. 1, Extended Data Fig. 2), providing unequivocal evidence for benthic life in the crater within years of the impact. Flattening of the structures indicates that the traces were formed while the sediment was still soft, during or shortly after deposition of the transitional unit. Infilling of the burrows with brown, fine-grained micrite also suggests traces were syndepositional and not derived from mixing of the Danian limestone above the transitional unit. Trace fossils produced during deposition of the limestone, as indicated by light infilling material, are distinct and only occur in the uppermost few cm of the transitional unit (Extended Data Fig. 2).

The transitional unit microfossils are dominated by clearly reworked Maastrichtian foraminifera and nannoplankton, known across the Gulf of Mexico and Caribbean as the K-Pg Boundary Cocktail<sup>19</sup> (Extended Data Fig. 3, Table S1). Although overall foraminiferal abundance (plotted as foraminifera per gram of sedimentary rock; Fig. 1) is high at the base

of the unit, species known to range across the boundary (“survivor species”) are rare in the lower transitional unit and become more common upsection even as total foraminifera decline (Fig. 1). Survivors, here defined as *Guembelitra cretacea*, *Muricohedbergella monmouthensis*, and *M. holmdelensis*<sup>20</sup>, dominate a depauperate assemblage in the upper 20 cm of the transitional unit, coinciding with the first appearance of trace fossils (Extended Data Figs. 4 and 5).

The nannofossil assemblage in the transitional unit contains reworked Cretaceous specimens, including a group of clearly overgrown species that became extinct near the Campanian-Maastrichtian boundary, such as *Aspidolithus parvus* and *Eiffellithus eximius*. The remainder of the Cretaceous species, which dominate the assemblage, range to the top of or beyond the latest Maastrichtian (Table S2). Unusually small (<2 µm) and delicate specimens of *Micula* are observed throughout the transitional unit and increase in abundance upsection (Fig. 1), along with small *Retecapsa* (Extended Data Fig. 6). Taxa common at other sites in the earliest Danian are also present, including disaster genera like *Thoracosphaera* and *Braarudosphaera*. Unlike the foraminifera, there are no clear stratigraphic trends in overall nannoplankton abundance (Fig. 1).

Because survivor species lived both before and after the K-Pg mass extinction, it is impossible to determine for certain if individual specimens in the transitional unit colonized the crater post-impact. However, the populations of foraminifera and nannoplankton are significantly different from those of the latest Cretaceous<sup>12</sup> (i.e., the expected population if the whole assemblage was reworked), suggesting that these taxa were true survivors (Fig. 1, Extended Data Fig. 6). *Guembelitra cretacea*, a common component of the survivor assemblage in the upper transitional unit, was restricted to marginal marine waters during the Maastrichtian and would not have been present at the pre-impact site, which was >100 m deep<sup>21</sup> and >500 km from shore<sup>22</sup>. The nannofossil assemblage in the transitional unit is significantly different from typical latest Maastrichtian assemblages, with some genera over-represented (*Watznaueria* and *Retecapsa*) and others under-represented (*Eiffellithus*, not including *E. eximius*, *Arkhangelskiella*, *Chiastozygus*, and *Prediscosphaera*) (Extended Data Fig. 6). Additionally, *Micula*, a robust taxon often used as a proxy for dissolution, is not as abundant as elsewhere, indicating that these unusual abundances are not due to poor or selective preservation (Extended Data Fig. 6).

This initial appearance of life is remarkably fast, especially because crater-specific factors do not seem to have had a negative impact on the local recovery of life. A vigorous, high-temperature hydrothermal system was established within the crater and may have persisted for millions of years after the impact<sup>23</sup>, especially across the peak ring where rocks exhumed from deep in the crust were extensively fractured<sup>7</sup>. Nevertheless, the appearance of burrowing organisms within years of the impact indicates that the hydrothermal system did not adversely affect seafloor life. Impact-generated hydrothermal systems are hypothesized to be potential habitats for early life on Earth<sup>24</sup> and on other planets, particularly below the surface. However, for marine impact craters in open ocean communication, like Chicxulub (Extended Data Fig. 1), our data indicate that locally significant but still comparatively small volumes of hydrothermal fluids were overwhelmed by the  $1.3 \times 10^4$  km<sup>3</sup> of well-mixed ocean water that filled the basin.

Likewise, the open connection with the Gulf of Mexico prevented the development of anoxia in the crater. Our analyses of iodine to calcium ratios suggest that local dissolved oxygen was high and stable in Zone P $\alpha$  (Fig. 3). This is in contrast to the smaller (85-km wide) Eocene Chesapeake Bay impact crater in Virginia, USA, where anoxia due to restriction is attributed as the cause of delayed recovery of the benthic ecosystem on the crater floor<sup>25</sup>. This comparison suggests that the establishment of life within marine impact craters is controlled more by circulation (and thus crater geometry) than by the magnitude of the impact or global environmental effects.

The overlying pelagic limestone, which was deposited within Zone P $\alpha$  (30–200 kyr post impact) contains abundant evidence of high productivity in a thriving ecosystem. The planktic foraminifer assemblage in Zone P $\alpha$  is diverse and abundant (Fig. 3). Good preservation in the lowermost sample (34 cm) allowed the identification of over 60 species of benthic foraminifera, and benthics make up 12% of the assemblage at this level (Table S1). This percentage of benthics<sup>26</sup> and the overall benthic assemblage<sup>27</sup> are both typical of an upper to middle bathyal paleo water depth (~600–700 m)<sup>10,27</sup>. At this level, trace fossils increase in size, abundance, and diversity. The abundance and diversity of benthic organisms indicate that by ~30 kyr after the impact, seafloor conditions had returned to normal and sufficient organic matter flux existed to sustain a diverse, multilayer benthic community.

Conversely, the nannoplankton assemblage in the Danian limestone is dominated by *Braarudosphaera* and calcareous dinoflagellate cysts (e.g., *Thoracosphaera*), common disaster taxa in the early recovery interval. Large, foraminifer-sized calcispheres appear after ~100 kyr. Calcareous phytoplankton in the earliest Danian clearly represent a low-diversity, high-productivity bloom. Genera like *Neobiscutum* and *Prinsius*, common bloom taxa in the recovery interval at other Northern Hemisphere sites, do not become common until several meters higher in the section, >1 myr after the impact. Organic microfossils are completely absent from the study interval, likely due to poor preservation of organic material.

Geochemical paleoproductivity proxies, particularly Ba/Ti and Ba/Fe ratios, also indicate high productivity in the post-impact Danian limestone (Fig. 1). Ba/Ti ratios of ~1.0 at the base of the limestone (~30 kyr post impact) and ~2.0 above that (15 cm higher or ~100 kyr post impact) indicate relatively high and increasing productivity in the Chicxulub Basin in the earliest Danian.

The recovery of productivity in the crater is faster than at many sites, including those in the Gulf of Mexico, some of which took 300 kyr or more to recover to a similar extent<sup>8,11</sup>. Therefore, we find that proximity to the impact was not a control on recovery in marine ecosystems. The wide range of rates of recovery in the oceans show no relationship with geographic distance to the crater and so are best explained by natural ecological interactions between organisms within recovery ecosystems like incumbency and competitive exclusion<sup>8,14</sup>. These trends can be used to understand the rates of recovery after other major extinction events and, critically, predict the long-term recovery of modern ecosystems affected by pollution and climate change.

## Methods

IODP-ICDP Expedition 364 drilled the peak ring of the Chicxulub crater in the spring of 2016 (Extended Data Fig. 1). Samples were taken at the Bremen IODP Core Repository during the Exp. 364 sampling party. Core depth in centimeters, with zero at the top of the section (616.24 m below sea floor), are reported throughout. Core material was indurated, and ~0.5 cm quarter-rounds were cut out with a rock saw. Due to the need to reserve core material for rare earth element geochemistry (which will be presented in a separate manuscript), the lowermost ~1.5 cm of the Danian limestone was not sampled. Individual samples were subdivided for foraminifer, calcareous nannoplankton, and discrete geochemical analyses.

Forty-three samples were examined for planktic and benthic foraminifera from Core 40 from 0–110 cm depth. Samples were weighed, crushed with a mortar and pestle, soaked overnight (or longer) in a 10% solution of hydrogen peroxide buffered with borax, and washed over a 43  $\mu\text{m}$  sieve to ensure capture of small Danian taxa. The sieve was soaked in methylene blue dye between samples to identify contaminated specimens. Samples were then dried in an oven, split to obtain a manageable volume of material, and examined for foraminifera, calcispheres, and other sand-sized particles. In the Danian limestone, at least 300 specimens were counted to establish a statistically robust population<sup>28</sup> and the rest of the residue was then examined for biostratigraphically significant taxa. Low abundances in the transitional unit precluded 300 specimen counts. However, we demonstrate that our values are sufficient to reject the null hypothesis (that the observed enrichments in survivor taxa are the result of random noise) with binomial confidence limits. This calculation traditionally provides the basis for the 300-specimen “rule:” counting 300 specimens provides statistical confidence at a 95% confidence interval that a species that makes up 1% of the population is represented in the count<sup>28</sup>. As we show, fewer specimens are sufficient to demonstrate the presence of a survivor population in our samples. Binomial confidence limits for samples with fewer than 300 specimens are reported in Table S1. Additionally, a single unusually well-preserved sample at the base of the post-impact limestone was examined for rare benthic species to determine the true diversity of benthics at the base of the unit (Table S1). Planktic foraminifer biozonation follows the P Zones of Berggren and Pearson<sup>29</sup> as modified by Wade et al.<sup>18</sup>.

Ninety-seven samples were examined for nannofossils. Samples were disaggregated in water and smear slides were made from the supernatant. Slides were observed in a transmitted light microscope at 1600 $\times$  until at least 100 specimens were observed (Table S2). Standard taxonomy was applied (<http://www.mikrotax.org/Nannotax3/index.php?dir=Coccolithophores>). The abundance of taxa at Site M0077 was compared to the global K-Pg nannoplankton compilation of Jiang et al.<sup>12</sup>.

Ichnological analysis was conducted from 0–110 cm. Ichnological observations were conducted on core material and a detailed and continuous analysis of digital images. To improve visibility of ichnological features, images were treated by a digital image methodology, based on modification of image adjustments as levels, brightness and vibrance<sup>30,31</sup>. Ichnotaxonomical classification of trace fossils was based on the overall shape

and the presence of diagnostic criteria such as size and presence of branches<sup>32</sup>. Special attention was given to the infilling material of biogenic structures.

The measurement of I/(Ca+Mg) was carried out using a procedure similar to that described by Lu et al.<sup>33</sup>. For each sample and geostandard approximately 3–4 mg of carbonate powder was weighed out, dissolved in ~0.45M nitric solution, and then diluted using 0.1M nitric acid and 0.5% TMAH solution. All reported measurements are with samples that had a matrix of  $50 \pm 5$  ppm Ca solution to ensure the most precise iodine measurement. Dissolved samples had TMAH solution added within an hour to avoid any possible loss of volatilized iodine<sup>33</sup>. Samples were measured using an Agilent inductively coupled plasma mass spectrometer 7500cs housed within the geochemistry group of the National High Magnetic Field Laboratory at Florida State University. A previously reported known sample, Key Largo (KL 1-1) was used to ensure reliable reproducibility. Our value of 5.51  $\mu\text{mol/mol}$  was within error of the reported value of 5.55  $\mu\text{mol/mol}$  (46). Hardisty et al.<sup>34</sup> found that a generally low oxygen conditions correspond to ~2.6  $\mu\text{mol/mol}$  for I/(Ca+Mg). Values are reported in Table S3.

Section 1 of Core 40 was scanned with an AVAATECH XRF Core Scanner II at MARUM, Bremen, Germany during the onshore phase of Expedition 364 (Fig. 1). The split core was covered with a 4  $\mu\text{m}$  thick SPEX CertiPrep Ultralene foil to avoid contamination. XRF data was acquired with a Canberra X-PIPS silicon drift detector with 1550 eV resolution, a Canberra DAS 1000 digital spectrum analyzer, and an Oxford Instruments 50W XTF011 X-ray tube with rhodium target material. X-ray spectra were processed with WIN AXIL software from Canberra Erisys at a resolution of 12 mm and a step of 10 mm. Scans were conducted at different voltages to determine a range of element concentrations: 50 kV, with a beam current of 1 mA (Ba and Sr; average dead time of 5%), and 10 kV with a beam current of 0.15 mA (Al, Si, K, Ca, Ti, Fe, Mn, and S; average dead time of 11%). For each scan, sampling time was 20 seconds per spot.

<sup>3</sup>He is delivered to the Earth's surface by cosmic dust grains and over short time spans (~Myr) can be used as a constant flux proxy<sup>35</sup>. Previous work has shown that the K-Pg impactor was not associated with enhanced <sup>3</sup>He flux, and the mean extraterrestrial <sup>3</sup>He flux from cosmic dust accretion at the end of the Cretaceous ( $106 \times 10^{-15}$  cc STP/g/cm<sup>2</sup>/kyr) was used to estimate the duration over which the K-Pg boundary clay was deposited at Gubbio and El Kef<sup>36</sup>. We use a similar approach here to establish the sedimentation rate of the transitional unit, which we use to develop an age model.

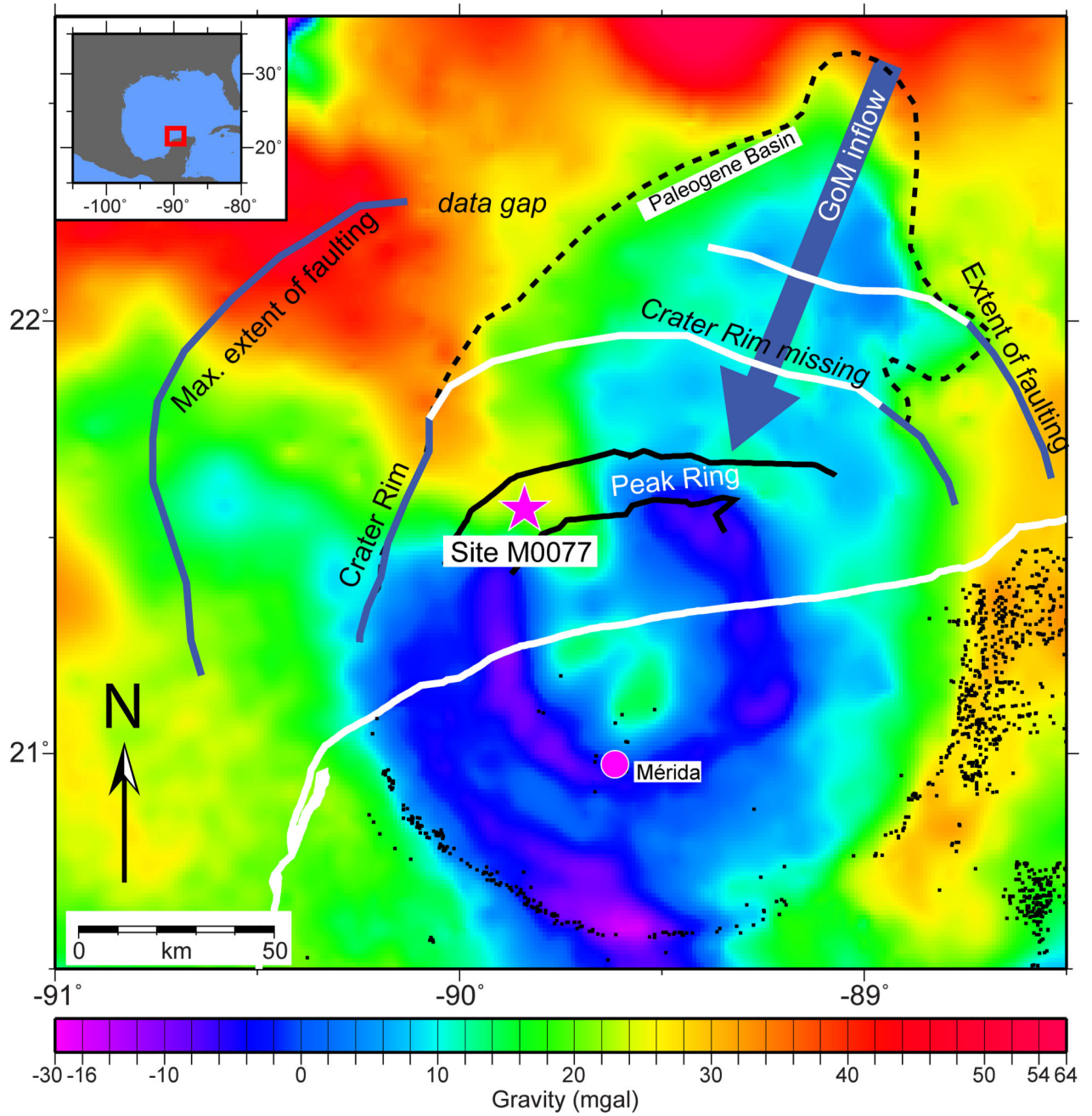
Helium isotope ratios and concentrations were measured on ~1g aliquots of sediment following standard analytical procedures<sup>31</sup>. Extraterrestrial <sup>3</sup>He concentrations were computed from measured He isotopic compositions using an isotopic deconvolution model<sup>36</sup>. Results are shown in Extended Data Table 1. <sup>3</sup>He concentrations and <sup>3</sup>He/<sup>4</sup>He ratios are generally low compared to typical marine sediments of similar age<sup>37,38</sup>. Nevertheless, with the exception of the lowest sample in the transitional unit (106.5 cm), the fraction of <sup>3</sup>He attributable to an extraterrestrial source is high, ranging from ~0.70 to 0.96. The deepest sample has a similar <sup>3</sup>He concentration to other samples in the transitional unit,



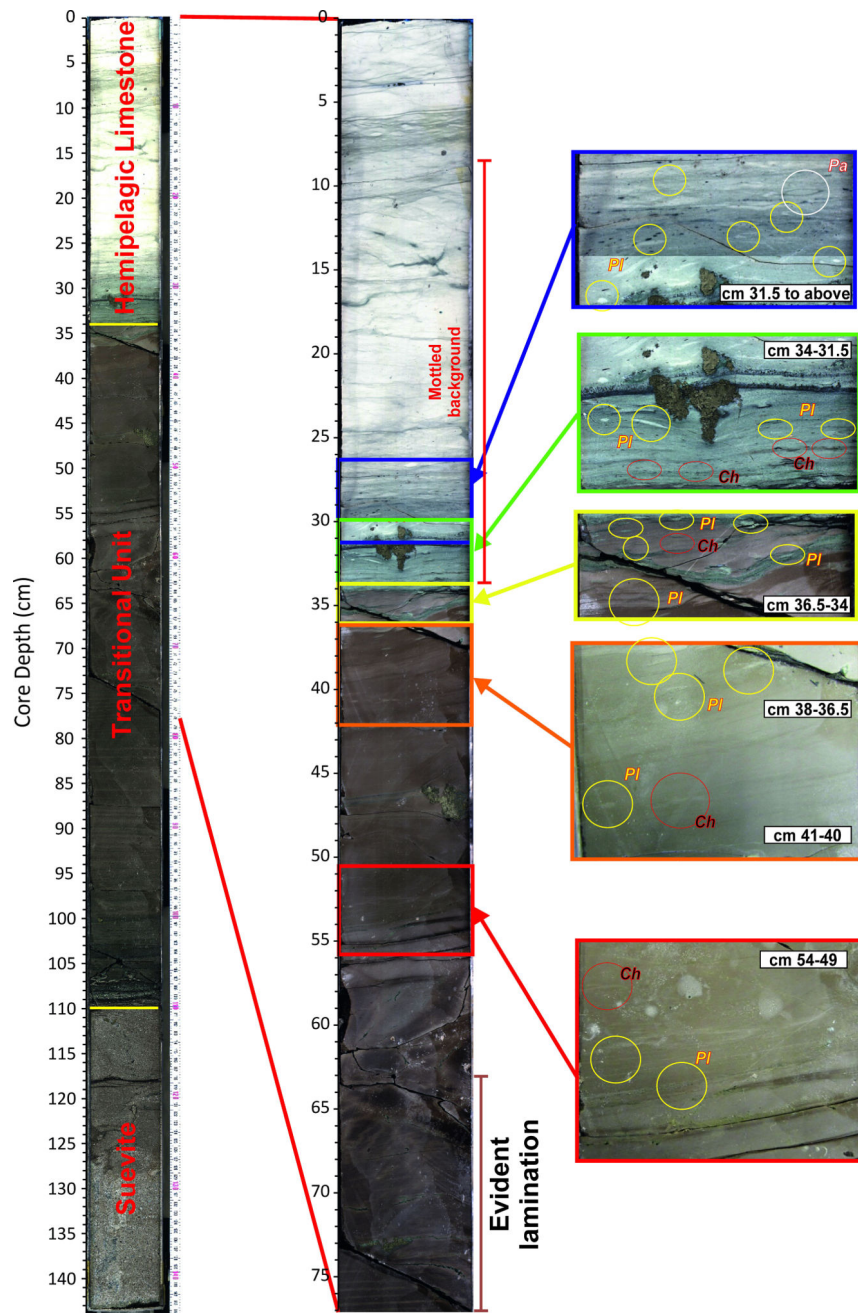
but ~5 times more  $^4\text{He}$ . This elevated  $^4\text{He}$  likely arises from a higher concentration of terrigenous  $^4\text{He}$ -bearing material deposited rapidly after the impact.

We see no evidence for extraterrestrial He carried in impactor fragments, such as highly elevated and/or highly variable  $^3\text{He}$  and  $^3\text{He}/^4\text{He}$  ratios. The absence of such a signal is consistent with either a) the absence of impactor fragments in the material analyzed, or b) loss of extraterrestrial  $^3\text{He}$  from the impactor via heating, vaporization or fusion. Note that, unlike many tracers of the impactor (such as Ir), deposition of fused or vaporized impactor will leave no trace in the sedimentary record because once He is lost into the atmosphere, it can no longer be retained in sediments.

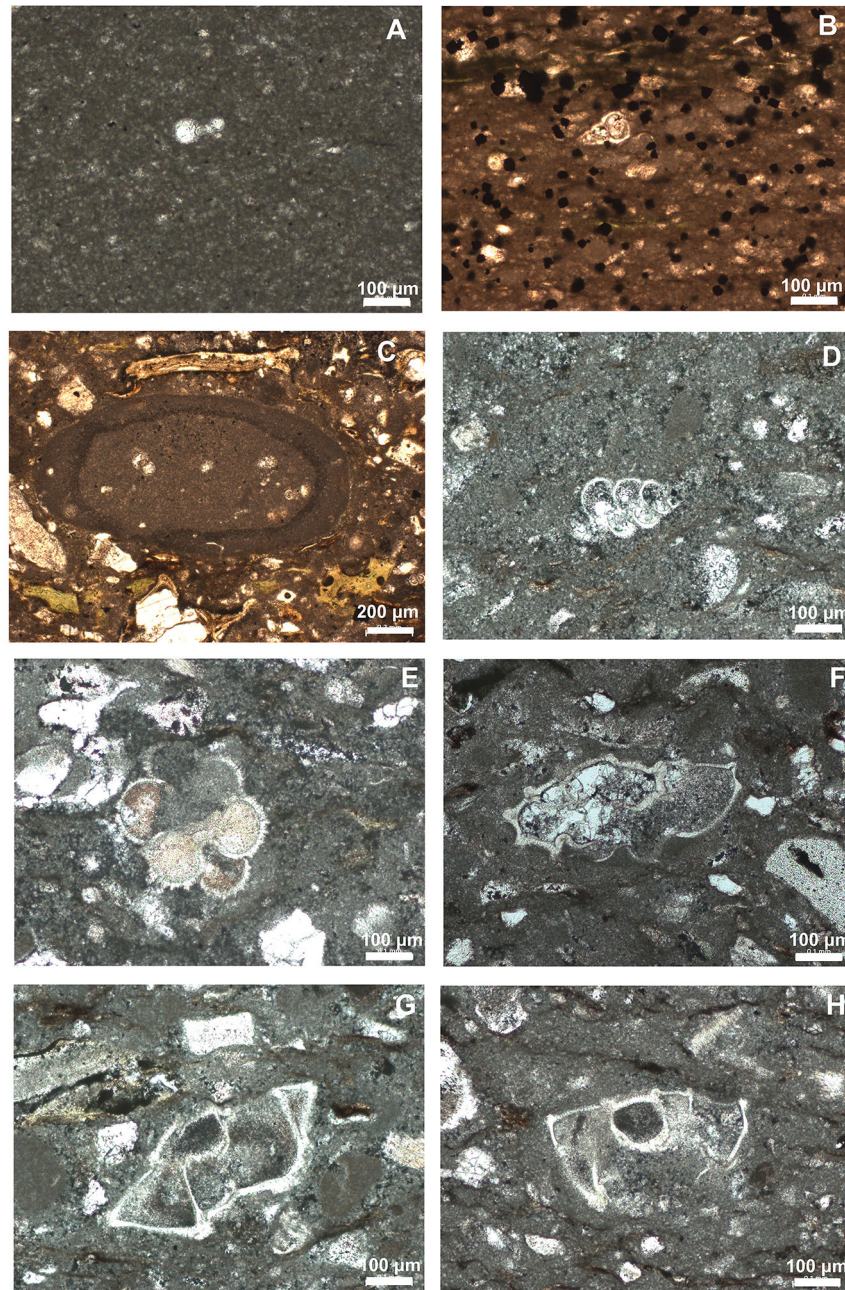
Extended Data



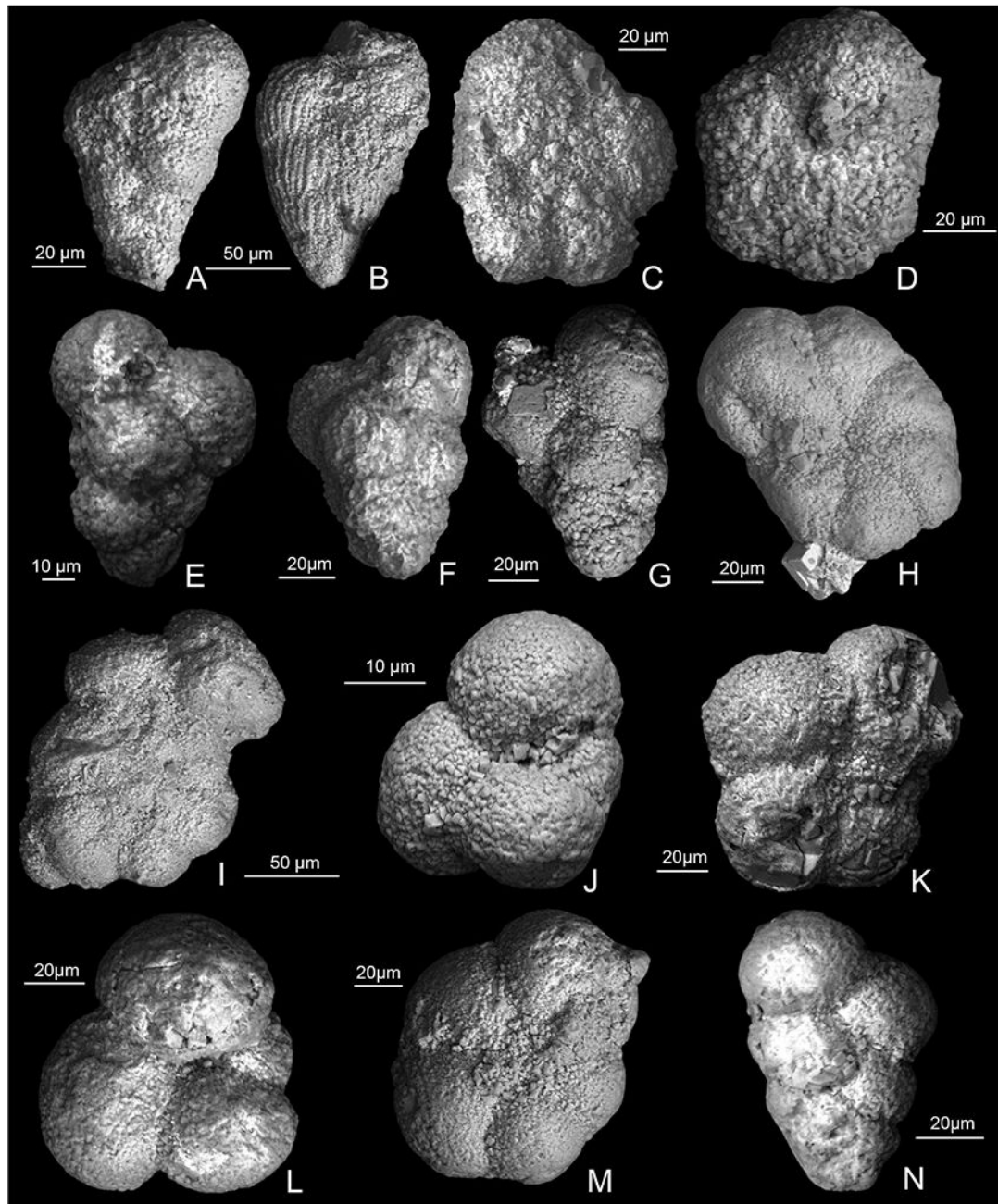
Extended Data Figure 1. Location of Site M0077 in the Chicxulub Crater as seen on gravity data. Black dots are cenotes. Modified from Gulick et al.<sup>21</sup>.



**Extended Data Figure 2. Trace fossils in Core 40 Section 1 of IODP Hole M0077A**  
 Discrete burrows in the upper transitional unit and the lower limestone are circled and labelled by the genus. Above the base of the limestone, trace fossils are abundant; representative examples are highlighted in the lower 10 cm of this interval. Ch: *Chondrites*; Pl: *Planolites*; Pa: *Paleophycus*.

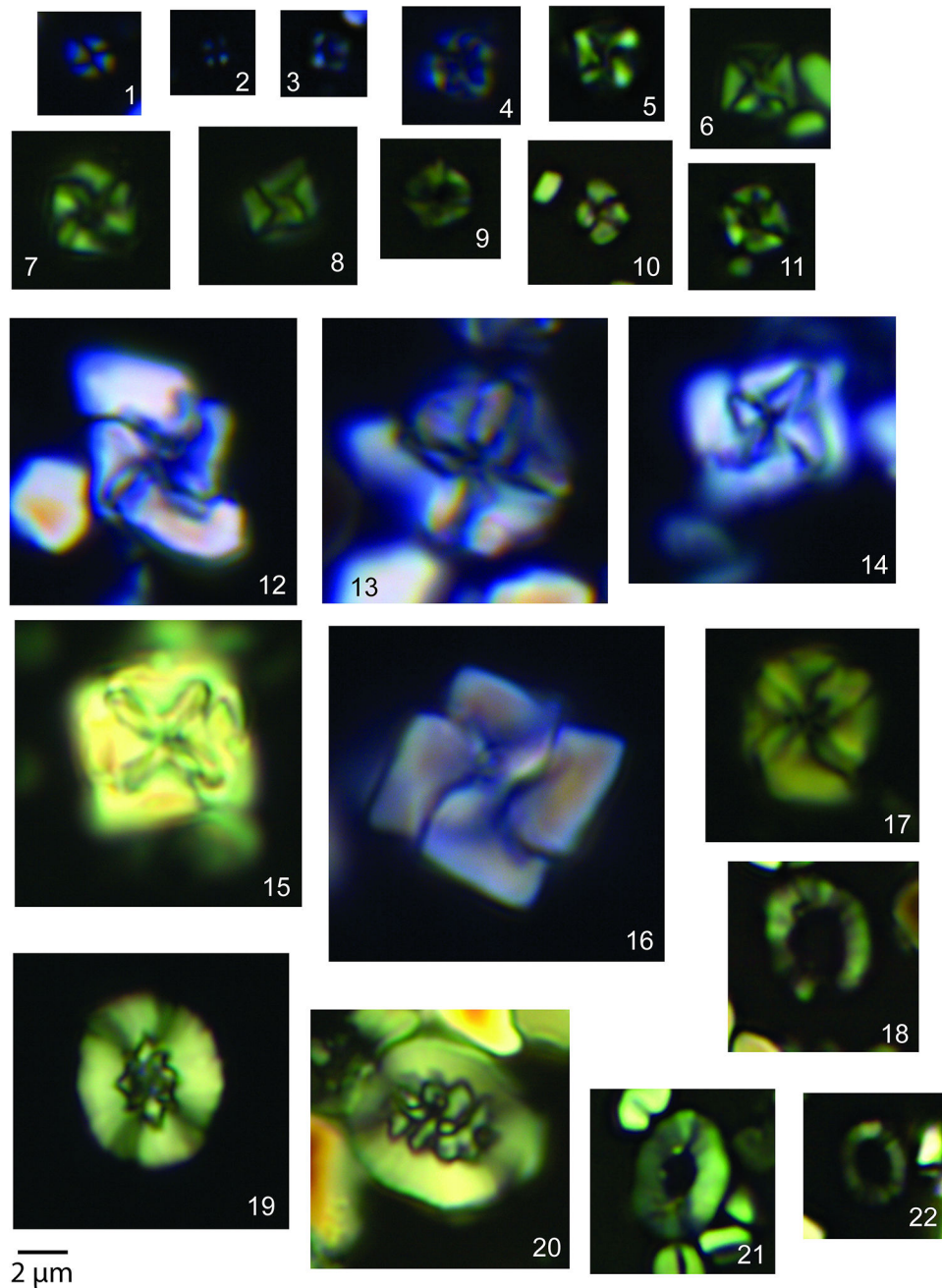


**Extended Data Figure 3. Reworked Cretaceous foraminifera in the transitional unit**  
**A** *Globigerinelloides* sp., 364-M0077A-40R-1-W 55–56 cm; **B** *Heterohelix* sp. 364-M0077A-40R-1-W 104–105 cm; **C** clast of pelagic limestone containing older Cretaceous planktic foraminifera 364-M0077A-40R-1-W 106–110 cm; **D** *Praegublerina pseudotessera* 364-M0077A-40R-1-W 118–129 cm; **E** *Racemiguembelina powelli* 364-M0077A-40R-1-W 118–129 cm; **F** *Globotruncana bulloides* 364-M0077A-40R-1-W 110–118 cm; **G** *Globotruncanita stuartiformis* 364-M0077A-40R-1-W 118–129 cm; **H** *Globotruncanita elevata* 364-M0077A-40R-1-W 118–129 cm. Scale bars are all 100 µm.



**Extended Data Figure 4. Scanning electron micrographs of planktic foraminifera from Core 40**  
**A–B**, examples of common reworked Cretaceous biserials, 364-M0077A-40R-1 102–103 cm; **C** *Muricohedbergella monmouthensis* 364-M0077A-40R-1-W 102–103 cm; **D** *Muricohedbergella holmdelensis* 364-M0077A-40R-1-W 44–45 cm; **E** *Guembelitra cretacea* 364-M0077A-40R-1-W 44–45; **F** *Guembelitra cretacea* 364-M0077A-40R-1-W 29–30 cm; **G** *Guembelitra cretacea* 364-M0077A-40R-1-W 29–30 cm; **H** *Parvularugoglobigerina eugubina* 364-M0077A-40R-1-W 31–32 cm; **I** *Parvularugoglobigerina eugubina* 364-M0077A-40R-1-W 31–32 cm; **J** *Globoconusa daubjergensis* 364-M0077A-40R-1-W 31–32 cm; **K** *Eoglobigerina eobulloides* 364-

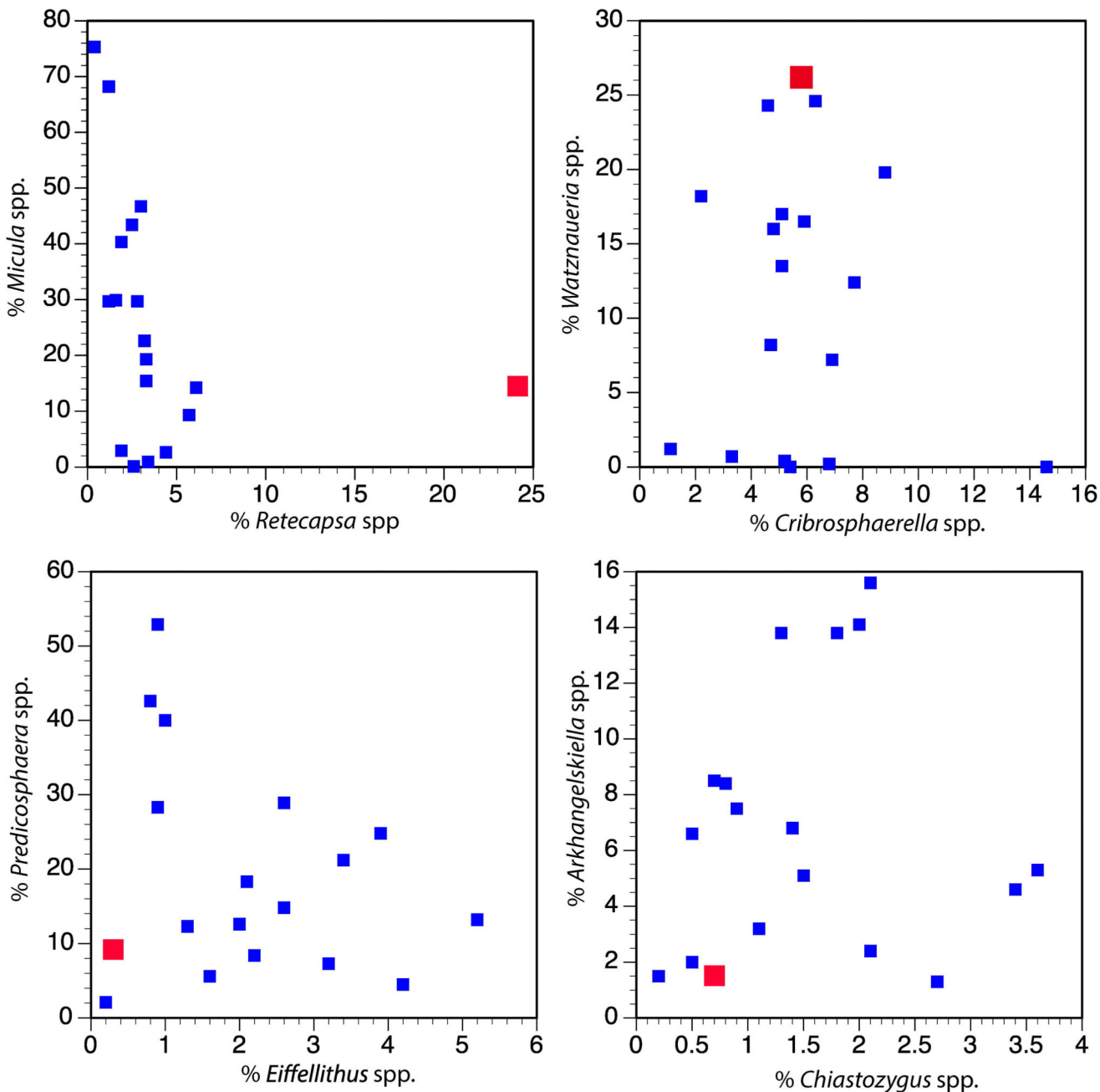
M0077A-40R-1-W 29–30 cm; **L** *Eoglobigerina edita* 364-M0077A-40R-1-W 29–30 cm; **M** *Praemurica taurica* 364-M0077A-40R-1-W 10–11 cm; **N** *Chiloguembelina morsei* 364-M0077A-40R-1-W 10–11 cm.



**Extended Data Figure 5. Small and regular sized nannofossils in the transitional unit**

All photographs from Core 364-M0077-40R-1-W. Plates 1–11, small *Micula* spp. 1. 55–56 cm; 2. 41–42 cm; 3. 95–96 cm; 4. 41–42 cm; 5. 90–91 cm; 6. 94–95 cm; 7. 91–92 cm; 8. 91–92 cm; 9. 45–46 cm; 10. 100–101 cm; 11. 81–82 cm. Plates 12–17 Regular-sized *Micula* spp. 12. 44–45 cm; 13. 41–42 cm; 14. 51–52 cm; 15. 105–106 cm; 16. 97–98 cm; 17. 36–37

cm. Plates 19–20 Regular-sized *Retecapsa* spp. 19. 85–86 cm; 20. 100–101 cm. 18, 21, 22 Small *Retecapsa* spp. 21. 71–72 cm, 22. 100–101 cm, 18. 100–101 cm. Scale bar is 2  $\mu$ m.



**Extended Data Figure 6. Relative abundance of major Maastrichtian calcareous nannoplankton** Small blue squares are Maastrichtian sites from the global compilation<sup>12</sup>; larger red squares are from the transitional unit at Site M0077. These data demonstrate the unusual abundance of *Watznaueria* and *Retecapsa* at our site.

Extended Data Table 1

<sup>3</sup>He data.

Sample	start cm	stop cm	<sup>3</sup> He pcc/g	<sup>4</sup> He ncc/g	Absolute <sup>3</sup> He/ <sup>4</sup> He	Fraction <sup>3</sup> He ET	Maximum <sup>3</sup> He -Based Model Age (kyr)
KT39	39	40	0.0068	13.6	5.04E-07	0.96	6.0
KT48	48	49	0.0055	35.4	1.56E-07	0.87	4.9
KT59	59	60	0.0064	23.1	2.78E-07	0.92	4.0
KT68	68	69	0.0042	31.6	1.33E-07	0.84	2.9
KT79	79	80	0.0036	18.3	1.99E-07	0.9	1.9
KT89	89	90	0.0105	34.7	3.04E-07	0.93	0.9
KT99	99	100	0.0045	64.3	6.99E-08	0.70	0.1
KT106.5	107	108	0.0109	327	3.32E-08	0.37	0.0

## Supplementary Material

Refer to Web version on PubMed Central for supplementary material.

## Acknowledgments

This research used samples and data provided by IODP. Expedition 364 was jointly funded by the European Consortium for Ocean Research Drilling (ECORD) and ICDP, with contributions and logistical support from the Yucatán State Government and Universidad Nacional Autónoma de México (UNAM). We thank Tessa Cayton for assistance crushing and washing samples; Serena Dameron, Renata Moura de Mello, and Mark Leckie for helpful discussions on benthic foraminifer taxonomy; James Maner for assistance with the UT ESEM laboratory and Rowan Martindale for assistance with petrographic microscope imaging. We are particularly grateful for assistance of the staff of the IODP Core Repository in Bremen, Germany for their assistance taking these samples and running “shipboard” analyses. The authors acknowledge Post-Expedition Awards from the U.S. Science Support Program for CL and TB, NSF OCE 1737351, and NASA NNX16AJ60G. Funding for FR-T was provided by Project CGL2015-66835-P (Secretaría de Estado de I+D+I, Spain), and Scientific Excellence Unit UCE-2016-05 (Universidad de Granada).

## References

- Jablonski D. Extinctions in the fossil record. In: Lawton JH, May RM, editors *Extinction Rates*. New York: Oxford University Press; 1995:2544
- Schulte P, et al. The Chicxulub asteroid impact and mass extinction at the Cretaceous-Paleogene Boundary. *Science*. 2010; 327:1214–1218. [PubMed: 20203042]
- Alvarez LW, Alvarez W, Asaro F, Michel HV. Extraterrestrial cause for the Cretaceous/Tertiary extinction. *Science*. 1980; 208:1095–1108. [PubMed: 17783054]
- Smit J, Hertogen J. An extraterrestrial event at the Cretaceous-Tertiary boundary. *Nature*. 1980; 285:198–200.
- Renne PR, et al. Time scales of critical events around the Cretaceous-Paleogene Boundary. *Science*. 2013; 339:684–687. [PubMed: 23393261]
- Hildebrand AR, et al. Chicxulub Crater: A possible Cretaceous/Tertiary boundary impact crater in the Yucatán Peninsula, Mexico. *Geology*. 1991; 19:867–871.
- Morgan J, et al. The formation of peak rings in large impact craters. *Science*. 2016; 354:878–882. [PubMed: 27856906]
- Hull PM, Norris RD. Diverse patterns of ocean export productivity change across the Cretaceous-Paleogene boundary: New insights from biogenic barium. *Paleoceanography*. 2011; 26:PA3205.



9. Alegret L, Thomas E. Cretaceous/Paleogene boundary bathyal paleo-environments in the central North Pacific (DSDP Site 465), the northwestern Atlantic (ODP Site 1049), the Gulf of Mexico, and the Tethys: The benthic foraminiferal record. *Palaeogeography, Palaeoclimatology, Palaeoecology*. 2005; 224:53–82.
10. Alegret L, Molina E, Thomas E. Benthic foraminifera at the Cretaceous-Tertiary boundary around the Gulf of Mexico. *Geology*. 2001; 29:891–894.
11. Alegret L, Arenillas I, Arz JA, Molina E. Foraminiferal event-stratigraphy across the Cretaceous/Paleogene boundary. *Neues Jahrbuch für Geologie und Paläontologie – Abhandlungen*. 2004; 231:25–50.
12. Jiang S, Bralower TJ, Patzkowsky ME, Kump LR, Schueth JD. Geographic controls on nannoplankton extinction across the Cretaceous/Paleogene Boundary. *Nature Geoscience*. 2010; 2010:280–285.
13. Solé RV, Montoya JS, Erwin DH. Recovery after mass extinction: evolutionary assembly in large-scale biosphere dynamics. *Philosophical Transactions of the Royal Society of London*. 2002; 357:697–707. [PubMed: 12079530]
14. Schueth JD, Bralower TJ, Jiang S, Patzkowsky ME. The role of regional survivor incumbency in the evolutionary recovery of calcareous nannoplankton from the Cretaceous/Paleogene (K/Pg) mass extinction. *Paleobiology*. 2015; 41:661–679.
15. Hull PM, Norris RD, Bralower TJ, Schueth JD. A role for chance in marine recovery from the end-Cretaceous extinction. *Nature Geoscience*. 2011; 4:856–860.
16. Yedid G, Ofria CA, Lenski RE. Selective press extinctions, but not random pulse extinctions, cause delayed ecological recovery in communities of digital organisms. *The American Naturalist*. 2009; 173:E1.
17. GulickSPS, , et al. Expedition 364 Preliminary Report: Chicxulub: Drilling the K-Pg Impact CraterInternational Ocean Discovery Program; 2017
18. Wade BS, Pearson PN, Berggren WA, Pälike H. Review and revision of Cenozoic tropical planktonic foraminiferal biostratigraphy and calibration to the geomagnetic polarity and astronomical time scale. *Earth Science Reviews*. 2011; 104:111–142.
19. Bralower TJ, Paull CK, Leckie RM. The Cretaceous-Tertiary boundary cocktail: Chicxulub impact triggers margin collapse and extensive sediment gravity flows. *Geology*. 1998; 26:331–334.
20. OlssonDK, , HemlebenC, , BerggrenWA, , HuberB. T, Atlas of Paleocene Planktonic ForaminiferaVol. 85. Smithsonian Contributions to Paleobiology; 1999
21. Gulick SPS, et al. Importance of pre-impact crustal structure for the asymmetry of the Chicxulub impact crater. *Nature Geoscience*. 2008; 1:131–135.
22. Sohl N. Upper Cretaceous. *Geology of North America, Volume J. Gulf of Mexico Basin*. 1991:205–244.
23. Abramov O, Kring DA. Numerical modeling of impact-induced hydrothermal activity at the Chicxulub crater. *Meteoritic and Planetary Science*. 2007; 42:93–112.
24. Cockell CS. The origin and emergence of life under impact bombardment. *Phil. Trans. R. Soc. B*. 2006; 361:1845–1856. [PubMed: 17008223]
25. PoagCW. Paleoenvironmental recovery from the Chesapeake Bay bolide impact: The benthic foraminiferal record. In: GohnGS, KoeberlC, MillerKG, , ReimoldWU, editorsThe ICDP-USGS Deep Drilling Project in the Chesapeake Bay Impact Structure: Results from the Eyreville Core Holes, The Geological Society of America Special PaperVol. 458. 2009747773
26. Leckie RM, Olson HC. Foraminifera as proxies for sea level change on siliciclastic margins. *SEPM Special Publication*. 2003; 75:5–19.
27. Alegret L, Thomas E. Upper Cretaceous and lower Paleocene benthic foraminifera from northeastern Mexico. *Micropaleontology*. 2001; 47:269–316.
28. Buzas MA. Another look at confidence limits for species proportions. *Journal of Paleontology*. 1990; 64:842–843.
29. Berggren WA, Pearson PN. A revised tropical and subtropical Paleogene planktonic foraminiferal zonation. *Journal of Foraminiferal Research*. 2005; 35:279–298.
30. Dorador J, Rodríguez-Tovar F. Digital image treatment applied to ichnological analysis of marine core sediments. *Facies*. 2014; 60:39–44.

31. Dorador J, Rodríguez-Tovar FJ. Stratigraphic variation in ichnofabrics at the “Shackleton Site” (IODP Site U1385) on the Iberian Margin: Paleoenvironmental implications. *Marine Geology*. 2016; 377:118–126.
32. Knaust D. *Atlas of Trace Fossils in Well Core: Appearance, Taxonomy and Interpretation* Springer; 2017
33. Lu Z, Jenkyns HC, Rickaby REM. Iodine to calcium ratios in marine carbonate as a paleo-redox proxy during oceanic anoxic events. *Geology*. 2010; 38:1107–1110. DOI: 10.1130/g31145.1
34. Hardisty DS, et al. Perspectives on Proterozoic surface ocean redox from iodine contents in ancient and recent carbonate. *Earth and Planetary Science Letters*. 2017; 463:159–170. DOI: 10.1016/j.epsl.2017.01.032
35. Farley KA, Eltgroth SF. An alternative age model for the Paleocene-Eocene thermal maximum using extraterrestrial  $^3\text{He}$ . *Earth and Planetary Science Letters*. 2003; 208:135–148.
36. Patterson DB, Farley KA. Extraterrestrial  $^3\text{He}$  in seafloor sediments: Evidence for correlated 100 kyr periodicity in the accretion rate of interplanetary dust, orbital parameters, and Quaternary climate. *Geochimica et Cosmochimica Acta*. 1998; 62:3669–3682.
37. Mukhopadhyay S, Farley KA, Montanari A. A 35 Myr record of helium in pelagic limestones from Italy: Implications for interplanetary dust accretion from the early Maastrichtian to the middle Eocene. *Geochimica et Cosmochimica Acta*. 2001a; 65:653–669.
38. Mukhopadhyay S, Farley KA, Montanari A. A short duration of the Cretaceous-Tertiary boundary event: Evidence from extraterrestrial Helium-3. *Science*. 2001b; 291:1952–1955. [PubMed: 11239153]

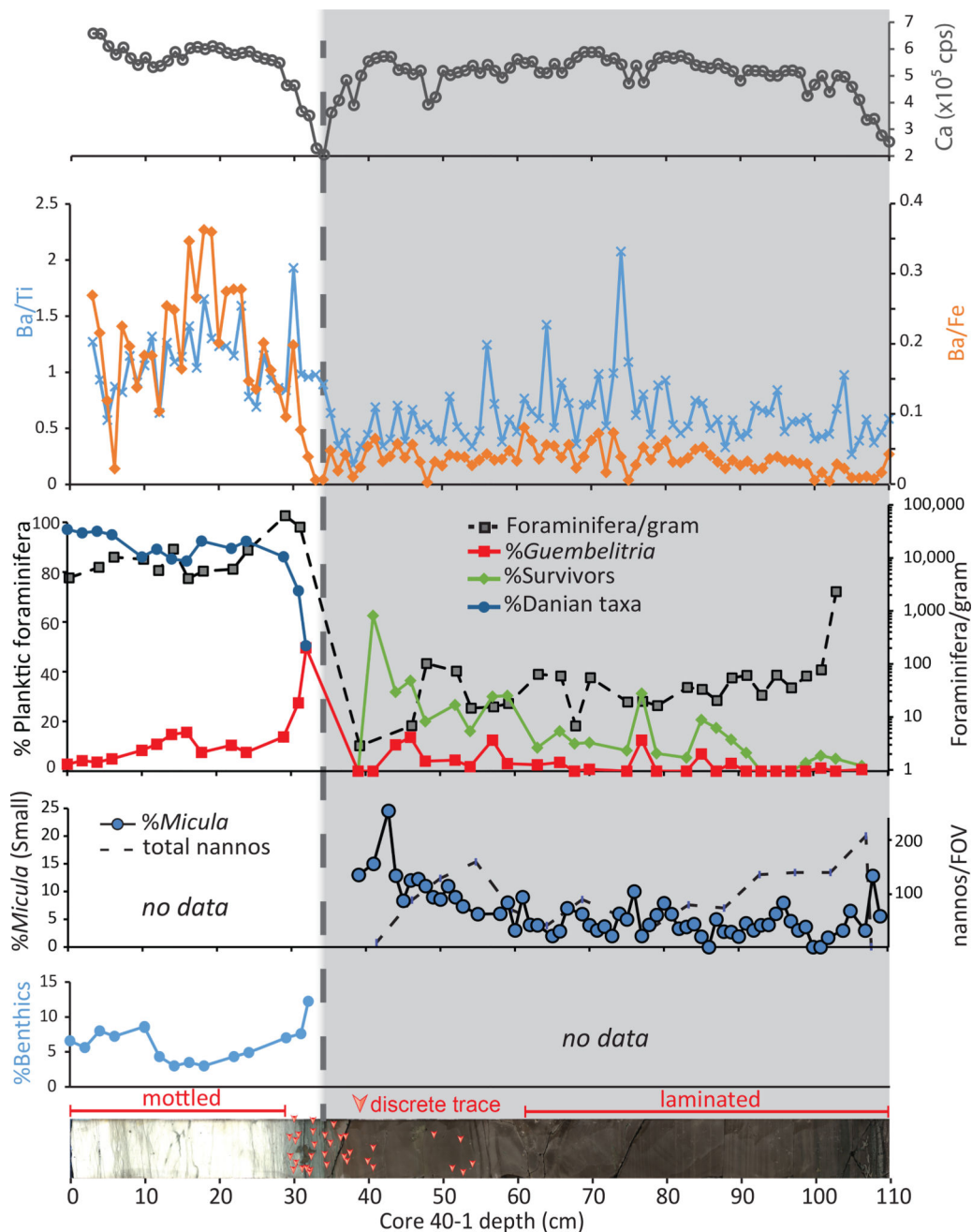


**Fig. 1. Paleoproductivity indicators in the earliest Paleocene at Site M0077**

The shaded area is the transitional unit and the dashed line represents the contact with the overlying pelagic limestone. Top to bottom: XRF-derived calcium abundance in counts per second (cps); Ba/Ti and Ba/Fe ratios; % abundances key planktic foraminiferal groups, including % *Guembelitra*, %survivors (i.e., Cretaceous species known to survive the impact), and % Danian taxa (i.e., species which evolved after the impact), as percentage of total foraminifera; foraminifera per gram of sediment, plotted on a log scale; % *Micula* smaller than 2µm (against total nannoplankton) and nannoplankton abundance (total occurrences per field of view – FOV); %benthic foraminifera (against total foraminifera); Core image of

364-M0077A-40R-1 0–110 cm Core 40R-1, 34 to 110 cm (616.58 to 617.33 meters below seafloor) with discrete trace fossils highlighted by arrows (see Extended Data Fig. 2 for larger version of this image).

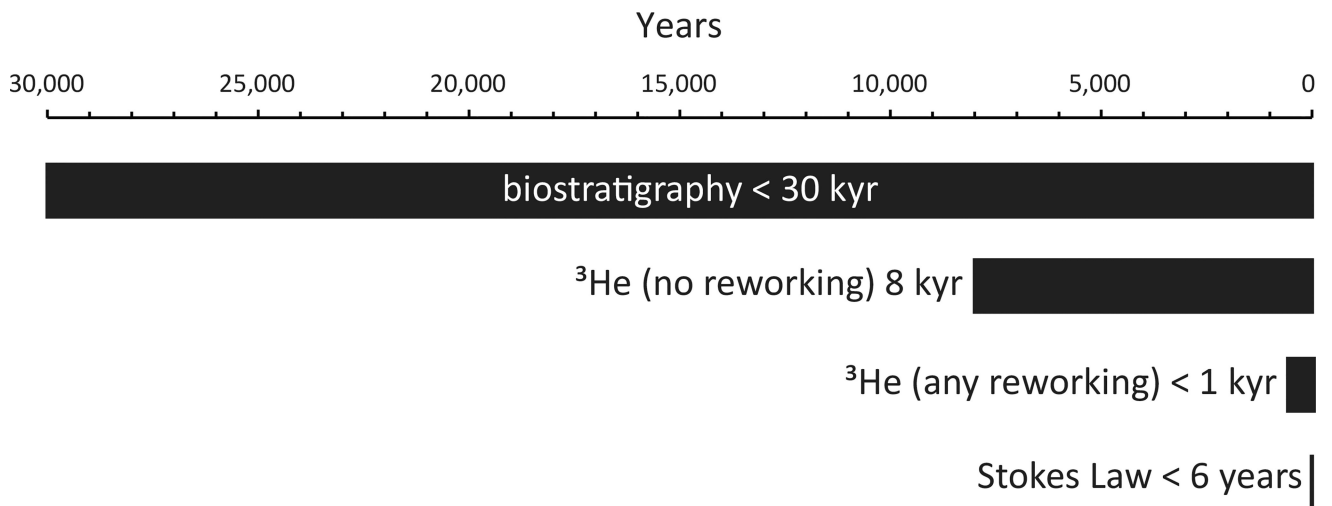
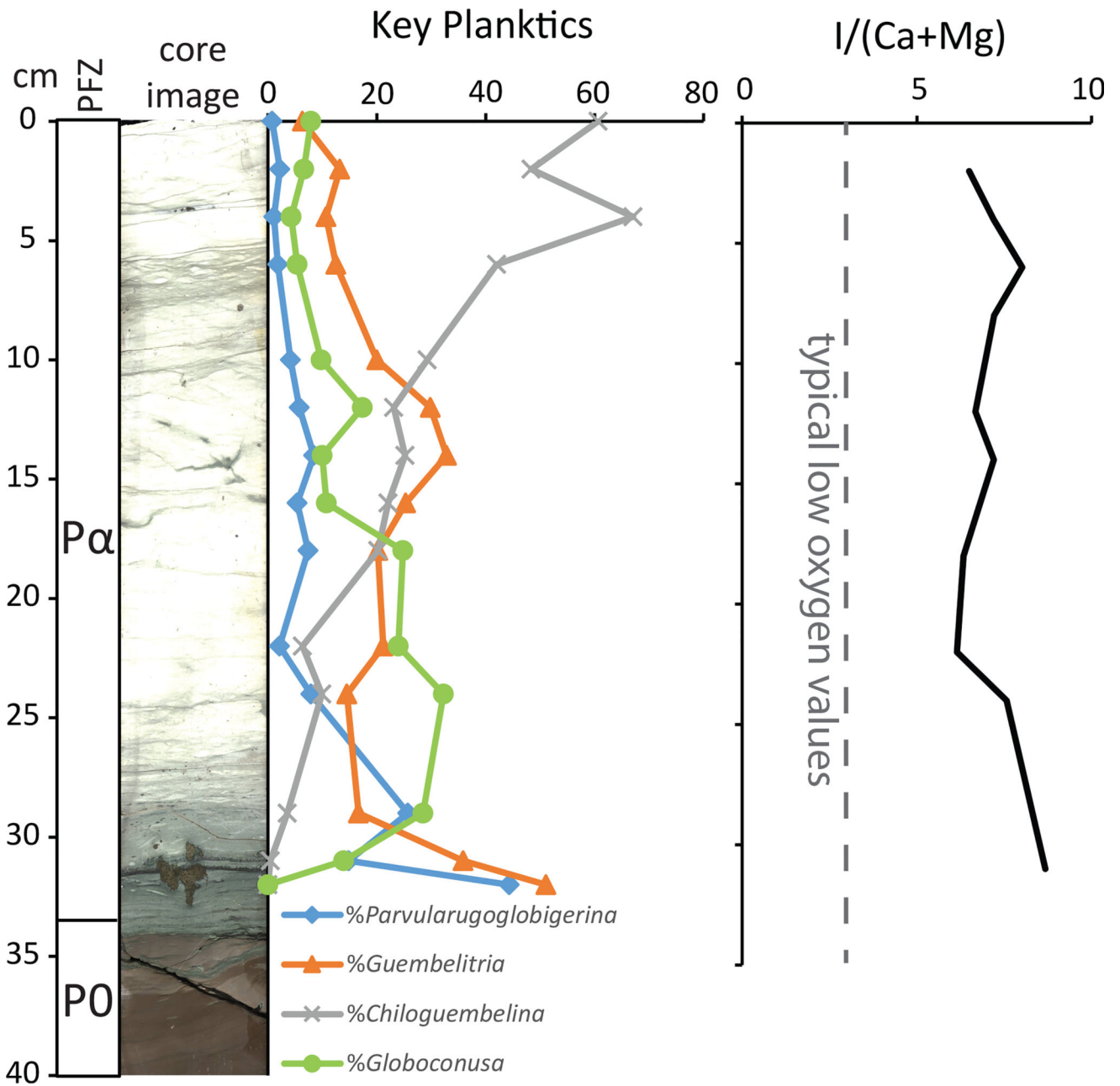


Figure 2. Constraints on the age of the transitional unit



**Figure 3. Early Danian foraminifer abundances and I/(Ca+Mg) oxygenation proxy**  
 Left: Key Danian planktic foraminifera. Normal perforate planktics (*Eoglobigerina*, *Globanomalina*, *Parasubbotina*, and *Praemurica*) are rare throughout the study interval and not plotted here; all are plotted as % total planktic foraminifera. Right: I/(Ca+Mg) redox proxy, indicating well-oxygenated conditions in the Chicxulub crater through this interval.